ACS Partner Journal

Journal of the American Society for Mass Spectrometry

pubs.acs.org/jasms

Article

Photochemical and Collision-Induced Cross-Linking of Asp, Glu, Asn, and Gln Residues in Peptide-Nitrile Imine Conjugate Ions in the Gas Phase

Mikuláš Vlk, Jiahao Wan, Marianna Nytka, Tuan Ngoc Kim Vu, Karel Lemr,* and František Tureček*

Cite This: *J. Am. Soc. Mass Spectrom.* 2025, 36, 175−186

Read Online

ACCESS | Metrics & More | Article Recommendations | Supporting Information

ABSTRACT: Peptide conjugates furnished with a 2,5-diaryltetrazolecarbonyl tag at the C-terminal lysine, which we call peptide-*tet*-K, were found to undergo efficient cross-linking of Asp, Glu, Asn, and Gln residues to transient nitrile-imine intermediates produced by photodissociation and collision-induced dissociation (CID) of the tetrazole ring in gas-phase ions. UV photodissociation (UVPD) at 213 nm achieved cross-linking conversion yields of 37 and 61% for DAAAK-*tet*-K and EAAAK-*tet*-K, respectively. The yields for NAAAK-*tet*-K and QAAAK-*tet*-K were 29 and 57%, respectively. Even higher cross-link yields were found for CID-MS^3 of stable denitrogenated ions, (peptide-*tet*-K−N_2 + H)$^+$, that were in the 69−83% range. Different types of cross-links were distinguished by CID-MS^n that showed a distinct series of backbone fragment ions, loss of N-terminal groups, and loss of phenylhydrazine from the modified nitrile imines. The Asp and Glu side-chain carboxyl groups were major participants in cross-linking that resulted in proton and oxygen transfer to the nitrile imine group. Other types of cross-linking involved Asn and Gln $CONH_2$ groups and backbone amides. Cyclic ion mobility-mass spectrometry was used to separate NAAAK-*tet*-K and QAAAK-*tet*-K conformers and products of their collision-induced denitrogenation. Linear nitrile-imine and cross-linked ion structures were identified by comparing the experimental collision cross sections (CCS_{exp}) to those for structures obtained by combined Born−Oppenheimer molecular dynamics and density functional theory (DFT) calculations. The formation of cross-links was found to be energetically favorable and involved proton-facilitated nucleophilic attack at the nitrile-imine carbon atom.

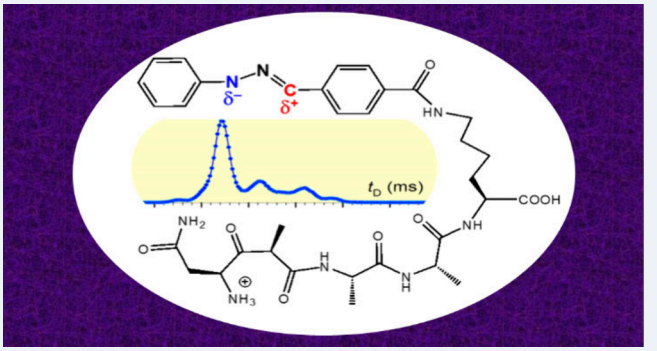

INTRODUCTION

Whereas nitrile imines represent well-known and used reactive intermediates in organic synthesis of pyrazolines and other heterocyclic compounds,[1,2] their use for covalent cross-linking and foot printing of biomolecules has been much less explored. Lin and co-workers have reported 2-aryl-5-carboxytetrazole-lysine analogues that have been found to cross-link to proximate nucleophile groups such as the Glu carboxyl in tagged proteins.[3,4] Cross-linking was initiated by the formation of nitrile-imine intermediates by photodissociative cleavage of the tetrazole ring, as shown for peptide-tetrazole conjugates (Scheme 1). More recently, Zhang, Li, and their co-workers have explored the reaction of tetrazoles with primary amines that, when accompanied by spurious oxidation in solution, led to cyclized triazole products. These authors have suggested that the new reaction involved nitrile-imine intermediates.[5] We have used photochemically and thermally generated nitrile-imine conjugates to achieve efficient cross-linking to peptides and dinucleotides in gas-phase ions.[6−8] Internal cross-linking in peptide-nitrile-imine conjugates has been found to produce novel macrocyclic peptide structures containing stable C−N bonds that are resistant to prototropic hydrolysis. This new class of structures complements the standard cyclopeptides that have been developed as peptidomimetics to target the so-called undruggable protein targets.[9] The specific feature of the gas-phase reactions that distinguished them from condensed-phase nitrile-imine reactions was that they were driven by the substantial internal excitation that was acquired by photon absorption. For example, loss of N_2 from tetrazole conjugates with peptides was calculated to have a low threshold energy, as shown in Scheme 1 for a NAAA-*tet*-K ion, leaving the nitrile-imine intermediate internally excited and promoting its intramolecular reactions resulting in covalent bond formation and cross-linking. In addition, the low threshold energy can be advantageous for the N_2 loss outcompeting peptide backbone

Received: September 23, 2024
Revised: November 19, 2024
Accepted: November 22, 2024
Published: November 28, 2024

Scheme 1. Formation of a Nitrile-Imine Intermediate as Exemplified by the $(NAAA\text{-}tet\text{-}K + H)^+$ Ion

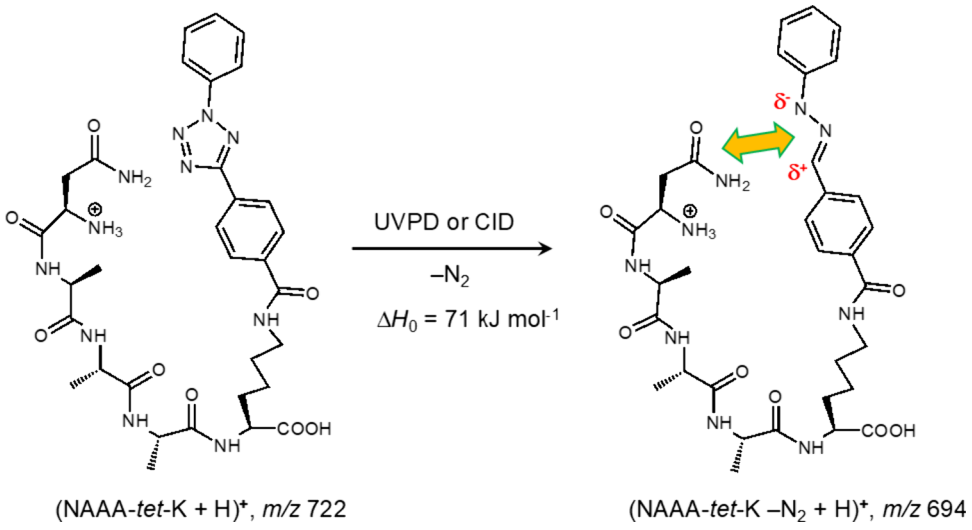

dissociations, which would allow use of CID for nitrile-imine generation. An important factor favoring cross-linking is the slow dissipation of internal energy to the environment under the low-pressure regime in the ion trap,[10−12] as opposed to much faster energy transfer in the condensed phase. The novel reactions were found to occur efficiently even in peptides that did not contain standard nucleophilic groups.[6,7] For example, the protonated conjugate of peptide GAAAK with the 2,5-diaryltetrazolecarbonyl substituent at the lysine side-chain amine, $(GAAA\text{-}tet\text{-}K + H)^+$, was converted to a transient nitrile imine in gas-phase ions that underwent cross-linking to the G-A amide group.[6] The reaction was found to be catalyzed by intramolecular proton transfer, based on experiments with gas-phase ions charged by sodium ion adduction that showed no cross-linking.[6] The initial study[6] posed several questions regarding the competitive reactivity of functional groups in amino-acid side chains and their specific reactivity toward the nitrile-imine group. In particular, acidic and basic amino acid residues and general nucleophiles have been of interest to further explore and potentially exploit these novel ion cross-linking reactions. To pursue these efforts, we now investigated UV photodissociation at 213 nm (UVPD) and CID of conjugate ions containing *N*-terminal Asp, Glu, Asn, and Gln residues in $(DAAA\text{-}tet\text{-}K + H)^+$, $(EAAA\text{-}tet\text{-}K + H)^+$, and their dimethyl esters $(D(OCH_3)AAA\text{-}tet\text{-}K(OCH_3) + H)^+$, $(E(OCH_3)AAA\text{-}tet\text{-}K(OCH_3) + H)^+$, $(NAAA\text{-}tet\text{-}K + H)^+$, and $(QAAA\text{-}tet\text{-}K + H)^+$.

The Asp and Glu residues can potentially react by the free carboxyl to form cross-links to the nitrile-imine group in a fashion analogous to condensed-phase cross-linking in proteins.[3,4] Effects of blocking the carboxyl proton as an amide or methyl ester are investigated with Asn, Gln, and esterified Asp and Glu residues. Our goal was to generate nitrile imines by UVPD and CID and use CID-MS^n to distinguish linear and cyclized reaction products. To characterize selected structures, we employed high-resolution ion mobility mass spectrometry and theoretical calculations, based on Born−Oppenheimer molecular dynamics and density functional theory, to obtain collision cross sections (CCS). We show that the carboxyl groups in Asp and Glu participate in efficient cross-linking to nitrile imines. Unexpectedly, cross-linking was also observed for the carboxamide groups in Asn and Gln.

EXPERIMENTAL SECTION

Materials and Methods. Peptide conjugates were synthesized on solid-support (Wang resin) by standard coupling procedures, starting with lysine side-chain derivatization with 4-(2-phenyl-2H-tetrazol-5-yl)benzoic acid, as described previously.[6] The peptide conjugates were characterized by high resolution mass spectrometry as ions obtained by protonation in electrospray. Accurate mass measurements are summarized in Tables S1−S4 (Supporting Information). Photodissociation at 250 nm (UVPD) and collision-induced dissociation of selected photoproducts from $(DAAA\text{-}tet\text{-}K)$ was performed on a Bruker amaZon 3D ion trap mass spectrometer as described previously.[13] The typical laser pulse energies at 250 nm were 1.8−2.0 mJ per pulse. UVPD spectra of all ions were obtained at 213 nm on an Orbitrap Ascend Tribrid instrument (ThermoFisher, San Jose, CA) with scanning the ion trap or in the high-resolution mode in the Orbitrap at 100 000 resolving power. Ion mobility measurements were carried out on a SELECT SERIES Cyclic Ion Mobility Spectrometer (c-IMS) (Waters Corp., Wilmslow, U.K.)[14] with direct infusion into a normal flow electrospray ion source at a flow rate of 5 μL/min. Each sample and calibrant were measured six times in positive mode. Typically, ion mobility separation over several cycles (n) was used at the total ion path of $n \times 98$ cm. Details of all measurement parameters and calibration for collision cross section (CCS) determination have been reported previously.[6]

Calculations. We used the previously developed protocol to obtain ion structures.[8] Briefly, this consisted of Born−Oppenheimer molecular dynamics (BOMD) calculations of 20 ps trajectories with 1 fs steps, using the Berendsen thermostat[15] at 510, 610, and 810 K, that were performed with PM6-D3H4[16] which complements the semiempirical Hamiltonian with dispersion and hydrogen-bonding interactions. These calculations were carried out using the high-end Cuby4 platform[17] and MOPAC.[18] Two hundred snapshots were selected at regular 100 fs intervals from each BOMD trajectory, and the structures were fully gradient-optimized with PM6-D3H4. Several low energy structures were selected and further

https://doi.org/10.1021/jasms.4c00394
J. Am. Soc. Mass Spectrom. 2025, 36, 175−186

optimized with B3LYP[19] with the 6-31+G(d,p) basis set, including empirical dispersion corrections (GD3-BJ).[20,21] All structures were established as local energy minima by harmonic frequency analysis. Several low-energy structures were selected and reoptimized with M06-2X[22] using the 6-31+G(d,p) basis set. The M06-2X/6-31+G(d,p) optimized geometries were used to calculate single-point energies which were carried out with M06-2X and the def2qzvpp[23] basis set (4200−4400 basis functions). Another set of M06-2X/6-31++G(d,p) single-point calculations were used to obtain charge densities according to Merz, Singh, and Kollman (MK).[24,25] All of the standard DFT calculations were run using Gaussian 16 (Revision B.01) that was licensed from Gaussian, Inc. (Wallingford, CT). Collision cross sections in nitrogen were calculated by the modified ion trajectory method (MobCal$_{MPI}$)[26,27] using the MK charge densities.

RESULTS AND DISCUSSION

DAAA-*tet*-K Spectra and Cross-Link Identification. CID and UVPD-MS^2 at 213 nm of the DAAA-*tet*-K ion ((DAAAK-*tet*-K + H)$^+$, m/z 723) resulted in a loss of N_2 from the tetrazole (m/z 695) that was accompanied by standard backbone cleavages forming a series of $[y_1 + 2H]^+$-$[y_4 + 2H]^+$ ions at m/z 395, 466, 537, and 608 (Figure 1a,b). For the standard fragment ions, we use the modified peptide ion nomenclature with explicit enumeration of hydrogen atoms and protons,[28] whereby y_n ions according to the Roepstorff-Fohlman system[29] are denoted as $[y_n + 2H]^+$. The loss of N_2 was more efficient on UVPD (Figure 1b), indicating the prevalent photochemical nature of this dissociation. In addition, even at the UVPD-MS^2 level the loss of N_2 was followed by the elimination of a HN═CH−CH_2COOH neutral fragment from the Asp residue. The resulting m/z 608 ion showed a doublet consisting of the $[y_4 + 2H]^+$ sequence ion as a minor component, and the major fragment ion due to the loss of $C_3H_5NO_2$, as established from the high-resolution CID-MS^2 spectrum (Figure 1a, inset). All fragment ion assignments were corroborated by accurate mass measurements and H/D exchange that provided the expected retention of deuterium in the fragment ions originating from the fully exchanged D_{10} precursor ion (Figure S1a−c, Supporting Information). For example, H/D exchange confirmed the loss of two deuterium atoms in $C_3H_3D_2NO_2$, indicating DN═CH−CH_2COOD assignment for the Asp side-chain fragment. Such a dissociation, which is highly uncommon in dissociations of straight-chain peptide ions, was analogous to aldimine losses from cross-linked peptide-tetrazole conjugates that were *N*-terminated with other amino acid residues (Gly, Ala), as reported earlier.[6] This dissociation indicated cross-linking to the nitrile imine at a position other than the Asp side-chain and amine group. Other uncommon fragment ions were found at m/z 527, 456, 385, 329, and 322 that were more abundant in the CID-MS^3 spectrum of the denitrogenated ion (m/z 695) that was generated by UVPD (Figure 1c). Very similar dissociations were found for CID-MS^3 of the (DAAAK-*tet*-K − N_2 + H)$^+$ ion that was generated by CID (Figure S2, Supporting Information). The Figure 1c and Figure S2 spectra showed two prominent series of fragment ions that were representative of cross-linked ion structures. Loss of internal Ala residues gave rise to ions at m/z 624, 553, and 482 (blue-annotated ions in Figure 1c) that indicated cross-linking by the *N*-terminal Asp residue to leave the Ala residues free for elimination. We denote these internal neutral fragments with square brackets, [Ala] to distinguish them from regular backbone fragments. The loss of internal residues is a hallmark of dissociations of cyclic peptides ions,[30,31] which in this case pointed to structures formed by cross-linking to the nitrile imine group. The other fragment ion series indicating cross-linking consisted of C-terminal ions carrying the Lys-attached $C_{14}H_{11}N_2O_2$ group that we denoted as υ_1-υ_3 (m/z 385, 456, 527, green-annotated ions in Figure 1c) to distinguish them from standard $[y_n + 2H]^+$ ions. Although, according to their formulas, the υ_n ions formally corresponded to water adducts to $[y_n + 2H]^+$ ions, we found them to be covalently bound. This was corroborated by the CID-MS^4 spectrum of the υ_3 ion (m/z 527) that showed backbone fragment ions by loss of [Ala] and [AlaAla], but only a very weak peak for loss of water that would have been expected as a major product from a noncovalent water adduct (Figure S3a, Supporting Information). Furthermore, the CID-MS^2 spectrum of (DAAAK-*tet*-K + H)$^+$ showed no $[y_n + 2H + H_2O]^+$ fragment ions (Figure 1a), confirming that the addition of water to $[y_n + 2H]^+$ ions did not occur as an ion−molecule reaction in the ion trap. Hence we conclude that the υ_n ions were covalently bound.

The formation and nature of the υ_n ions was further probed by obtaining a UVPD-CID-MS^3 spectrum of the DAAAK-*tet*-K dimethyl ester ((D(OCH_3)AAA-*tet*-K(OCH_3)−N_2 + H)$^+$, m/z

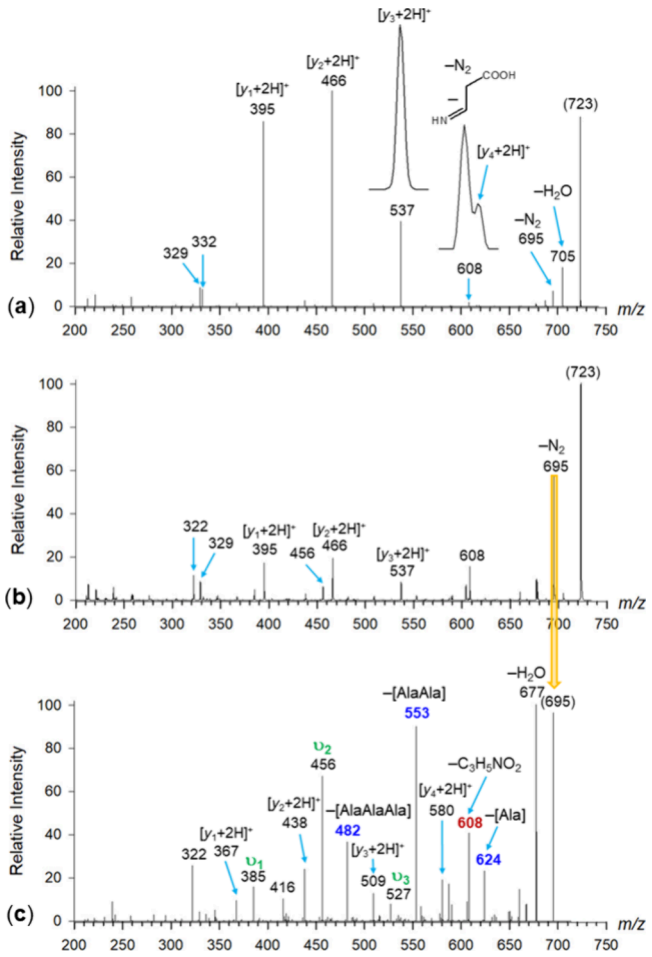

Figure 1. (a) CID-MS^2 spectrum of (DAAA-*tet*-K + H)$^+$ (m/z 723); (b) UVPD-MS^2 spectrum of (DAAA-*tet*-K + H)$^+$ (m/z 723) at 213 nm; (c) CID-MS^3 spectrum of (DAAA-*tet*-K − N_2 + H)$^+$ (m/z 695) generated by 213 nm UVPD of (DAAA-*tet*-K + H)$^+$.

https://doi.org/10.1021/jasms.4c00394
J. Am. Soc. Mass Spectrom. 2025, 36, 175−186

723) in which the Asp carboxyl was blocked (Figure 2a). The spectrum showed no υ_n ions, indicating that a free Asp

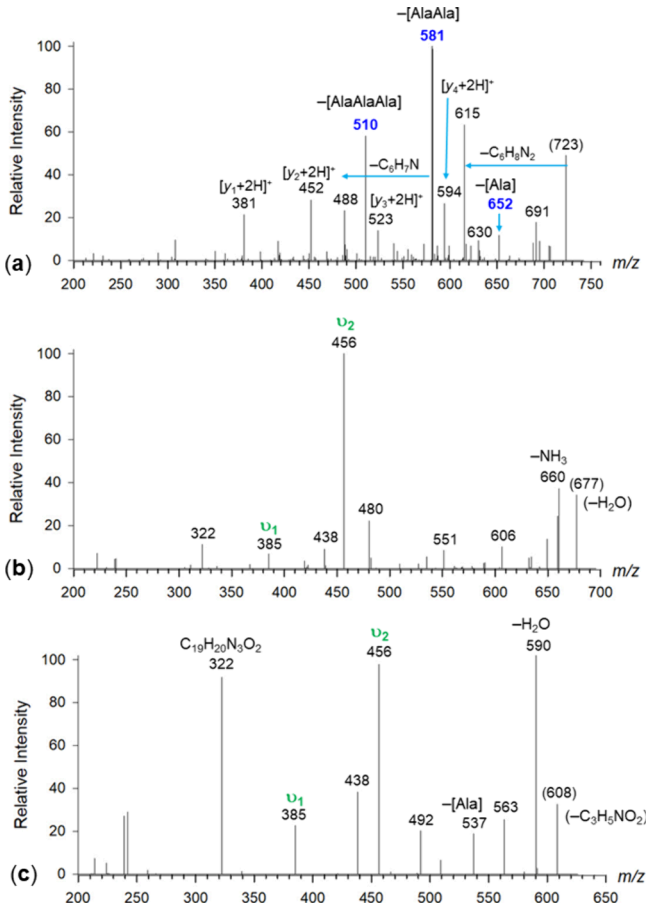

Figure 2. (a) UVPD-CID-MS^3 spectrum of (D(OCH$_3$)AAA-*tet*-K(OCH$_3$) − N$_2$ + H)$^+$ (m/z 723); (b) CID-MS^4 spectra of (b) m/z 677 and (c) m/z 608 ions from Figure 1c spectrum of (DAAA-*tet*-K − N$_2$ + H)$^+$.

carboxyl was required for this type of cross-linking. Despite the absence of υ_n ion formation from ((D(OCH$_3$)AAA-*tet*-K(OCH$_3$)−N$_2$ + H)$^+$, the Figure 2a spectrum did show loss of internal [Ala], [AlaAla], and [AlaAlaAla] residues, as visualized by the blue-annotated ions at m/z 652, 581 and 510, indicating cross-linked structures. Cross-linking in the methyl ester may involve the Asp amide, ester, or N-terminal amine group but did not result in oxygen transfer to the nitrile imine.

The formation of υ_n ions involving the carboxyl group can be viewed as proceeding from cross-links in which the Asp carboxyl proton was transferred to the negatively charged nitrile-imine nitrogen, and the electron-deficient carbon was attacked by the carboxyl oxygen forming a covalent C−O bond (Scheme 2). The formation of the υ_n fragment ions upon CID can be initiated by proton-promoted cleavage of the Asp CO−O bond, which can be assisted by participation of the amide oxygen forming a lactone intermediate. Further amide bond dissociations then led to the C-terminal υ_n ions in which the former Asp carboxyl oxygen and two hydrogen atoms were embedded in the nitrile imine moiety as a hydrazide (Scheme 2).

The formation of υ_n ions was also probed by CID-MS^4 of the m/z 677 (loss of water), and m/z 608 (loss of C$_3$H$_5$NO$_2$) primary fragment ions from the UVPD-CID-MS^3 spectrum of (DAAAK-*tet*-K + H)$^+$. Both of these CID-MS^4 spectra (Figure 2b,c) showed prominent υ_2 ions (m/z 456). Since the m/z 608 ion no longer had the Asp residue, the formation from it of the υ_2 ion indicated that the oxygen atom transferred to the nitrile imine can also originate from other accessible positions, e.g., the amide groups. Consistent with this, while carboxyl esterification stopped the formation of υ_n ions, it did not prevent internal backbone fragmentation, resulting in the loss of [Ala$_n$] that indicated cross-linked structures. The spectrum of the methyl ester further showed enhanced loss of C$_6$H$_8$N$_2$ (most likely phenyl hydrazine), giving the ion at m/z 615 that had only a minor homologue at m/z 587 in the CID-MS^3 spectrum of (DAAAK-*tet*-K + H)$^+$. Further CID-MS^4 of the m/z 615 ion (Figure S3b, Supporting Information) showed losses of internal [Ala] (m/z 544) and [AlaAla] (m/z 473), indicating that the ion was cross-linked when formed by the loss of phenylhydrazine. Overall, the DAAA-*tet*-K data showed that UVPD resulted in cross-linking to the nitrile imine, favoring (DAAAK-*tet*-K−N$_2$ + H)$^+$ structures dissociating to υ_n ions and methyl ester structures dissociating by loss of phenylhydrazine. The overall cross-link yields in the CID-MS^3 spectra were similar at 83% and 77% for (DAAAK-*tet*-K−N$_2$ + H)$^+$ and its methyl diester analogue, respectively (Table 1).

EAAA-*tet*-K Spectra and Cross-Link Identification. CID and UVPD of the homologous EAAA-*tet*-K ion ((EAAAK-*tet*-K + H)$^+$, m/z 737) gave different results (Figure 3a,b). CID resulted in regular backbone cleavages giving rise to standard [y$_n$ + 2H]$^+$ ions whereas loss of N$_2$ (m/z 709) was relatively less abundant, as were backbone υ_n fragment ions resulting from cross-linked nitrile-imine intermediates (Figure 3a). In contrast, UVPD gave a prominent series of υ_n ions (m/z 385, 456, 527, green-annotated ions in Figure 3a−c) in addition to the [y$_n$+2H]$^+$ ions (Figure 3b). Products of deep photodissociation containing an oxygenated nitrile imine moiety, such as C$_{19}$H$_{20}$N$_3$O$_2$ (m/z 322) and C$_{14}$H$_{11}$N$_2$O$_2$ (m/z 239) were also formed upon UVPD (Figure 3b). The differences can be ascribed to different modes of ion excitation. Slow heating on CID, resulting in ion vibrational excitation, chiefly promoted low-energy dissociations, such as peptide backbone cleavage, forming [y$_n$ + 2H]$^+$ ions without N$_2$ loss from the tetrazole group. In contrast, absorption of the 213 nm photon (561 kJ mol^{-1}) by the diaryltetrazole chromophore initiated tetrazole ring cleavage from an excited electronic state. Comparing the typical reaction enthalpy for the tetrazole N$_2$ loss (50−80 kJ mol^{-1})[6,7] with the 213 nm photon energy, one can expect the nitrile-imine intermediates formed by UVPD to be substantially excited. Further exothermic cross-linking with oxygen atom and proton transfer to the nitrile-imine intermediate can further energize the cross-links to trigger backbone cleavage.

The dissociations originating from cross-links were further emphasized in the CID-MS^3 spectrum of the (EAAAK-*tet*-K−N$_2$ + H)$^+$ ion (m/z 709), that was generated by UVPD (Figure 3c). The Figure 3c spectrum showed [y$_n$ + 2H]$^+$ ions at m/z 367, 438, 509, and 580 that were presumed to represent structures with a linear peptide chain. In addition, ions formed by internal losses of [Ala$_n$], indicating cross-linked structures, were prominent at m/z 638, 567, and 496. Another ion series pointing to cross-links by the Glu carboxyl was represented by υ_n ions at m/z 527, 456, and 385. We note that the CID-MS^3 spectrum of the (EAAAK-*tet*-K−N$_2$ + H)$^+$ ion (m/z 709) that

https://doi.org/10.1021/jasms.4c00394
J. Am. Soc. Mass Spectrom. 2025, 36, 175−186

Scheme 2. Proposed Asp Carboxyl Cross-Linking Mechanism and Backbone Dissociations in the Cross-Links

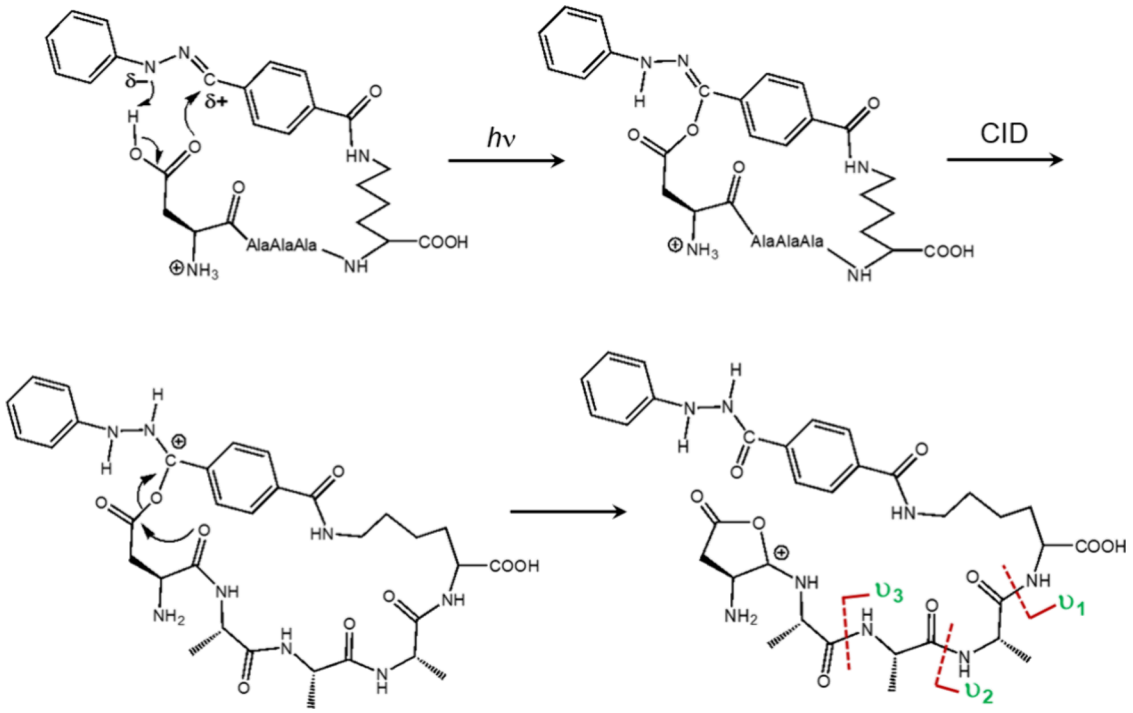

Table 1. Cross-Linking Yields

	CID-MS^3				
Cross-linking yield (%)[a]					
sequence	UVPD-MS^2	υ_n	Ala	$C_6H_8N_2$	total
DAAA-*tet*-K	37	35	44	5	83
D(OCH_3)AAA-*tet*-K(OCH_3)	50	2	44	31	77
EAAA-*tet*-K	61	40	34	6	80
E(OCH_3)AAA-*tet*-K(OCH_3)	62	2	40	25	67
NAAA-*tet*-K	29	4	52	16	72
QAAA-*tet*-K	57	23	37	9	69

[a]Sum of identified cross-link fragment ion intensities relative to the sum of all backbone fragment ion intensities. Ions by loss of water, ammonia, and combinations thereof that can originate from both linear and cross-linked isomers were not included.

was generated by CID was similar to the Figure 3c spectrum, showing identical fragment ions (Figure S4, Supporting Information).

We also investigated the effect on UVPD and CID of carboxyl methylation in EAAAK-*tet*-K dimethyl ester, as illustrated by the UVPD-CID-MS^3 spectrum of the denitrogenated ion at m/z 737 (Figure S5, Supporting Information). The spectrum showed a very minor formation of υ_n ions that were represented only by a weak υ_2 ion at m/z 470. Nevertheless, loss of phenylhydrazine (m/z 629) and internal [Ala$_n$] residues (m/z 666, 595, and 524) attested to a major fraction of cross-linked structures. Linear peptide structures were indicated by the standard $[y_n + 2H]^+$ ions at m/z 381, 452, 523, and 594. These figures were reflected by the cross-linking yields for EAAAK-*tet*-K and its dimethyl ester (Table 1). The cross-linking yields upon UVPD were very similar for EAAAK-*tet*-K and its dimethyl ester at 61% and 62%, respectively (Table 1). The cross-linking yields upon CID of denitrogenated ions were slightly higher for (EAAAK-*tet*-K −

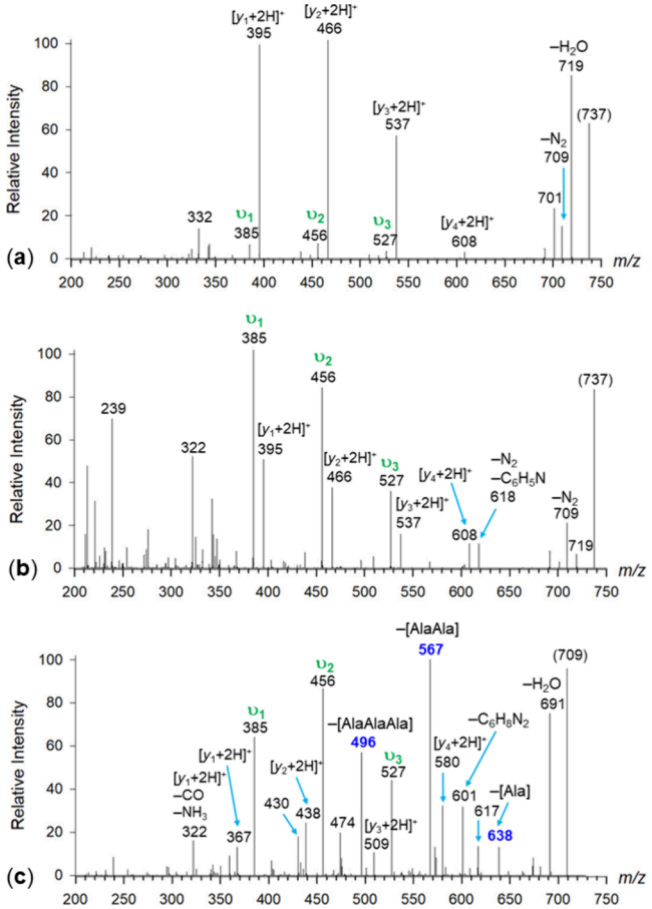

Figure 3. (a) CID-MS^2 spectrum of (EAAA-*tet*-K + H)$^+$ (m/z 737); (b) UVPD-MS^2 spectrum of (EAAA-*tet*-K + H)$^+$ (m/z 737) at 213 nm; (c) CID-MS^3 spectrum of (EAAA-*tet*-K − N_2 + H)$^+$ (m/z 709) generated by 213 nm UVPD of (EAAA-*tet*-K + H)$^+$.

https://doi.org/10.1021/jasms.4c00394
J. Am. Soc. Mass Spectrom. 2025, 36, 175−186

N_2 + H)$^+$ than for its methyl ester at 80% and 67%, respectively. The lower yield for the methyl ester was chiefly due to the near absence of υ_n ions. We presumed that the mechanism of the υ_n ion formation from EAAAK-*tet*-K was analogous to that shown in Scheme 2 and hinged on the availability of a free Glu carboxyl group.

NAAA-*tet*-K and QAAA-*tet*-K Spectra and Cross-Link Identification. The effect on cross-linking of the side-chain functional groups was further investigated with NAAA-*tet*-K and QAAAK-*tet*-K to provide a comparison of the side-chain amide groups with the corresponding carboxyl groups in DAAA-*tet*-K and EAAA-*tet*-K and their methyl esters. The UVPD-MS^2 spectra of (NAAA-*tet*-K + H)$^+$ (m/z 722) and (QAAA-*tet*-K + H)$^+$ (m/z 736) showed a series of $[y_n + 2H]^+$ ions in addition to the N_2 loss peaks at m/z 694 and 708, respectively (Figure S6a,b). Cross-linking upon UVPD was indicated by the common m/z 608 ion resulting from the loss of the respective N-terminal HN═$CHCH_2CONH_2$ and HN═$CHCH_2CH_2CONH_2$ neutral fragments from the Asn and Gln residues. These dissociations have also been observed for UVPD of the Asn and Gln conjugates at 250 nm which, however, resulted in less backbone dissociation.[6] The unusual dissociation of the C_α–CO bond in the Asn and Asp residues did not involve radical intermediates, as opposed to analogous backbone cleavages leading to x-type fragment ions in peptide cation radicals,[32,33] and upon peptide ion photofragmentation at 157 nm[34] and 192 nm.[35] Although the mechanism of this dissociation, involving the transfer of two hydrogens, was unknown, its occurrence pointed to cross-linking off the N-terminal residue.

Further information was obtained from CID-MS^3 of the denitrogenated ions (Figure 4a,b). The spectrum of (NAAA-*tet*-K–N_2 + H)$^+$ (m/z 694, Figure 4a) showed a major loss of ammonia (m/z 677) that was analogous to the loss of water from (DAAA-*tet*-K–N_2 + H)$^+$ (Figure 1c). Although ammonia and water could originate from various positions in the ions, the coincidence of their elimination from Asn and Asp, respectively, seemed to indicate they came from the carboxamide and carboxyl group. Note that loss of ammonia was not observed in UVPD-MS^2 of (NAAA-*tet*-K + H)$^+$ (Figure S6a), and its prominent presence in the CID-MS^3 spectrum of the denitrogenated ion suggested that it originated from cross-linked structures. The Figure 4a spectrum shows two series of backbone fragment ions. One was the $[y_n + 2H]^+$ ions at m/z 367, 438, 509, and 580 that we interpreted as markers of linear nitrile-imine structures. The other series involved losses of internal [Ala] residues, producing ions at m/z 481, 552, and 623 (blue-annotated ions). These unequivocally represented cyclic cross-linked ion structures. In addition, the spectrum displayed an m/z 586 ion by loss of $C_6H_8N_2$ (phenylhydrazine) and the m/z 608 ion due to loss of HN═$CHCH_2CONH_2$. CID-MS^4 of the latter ion (Figure 4c) showed dominant υ_2 and υ_1 ions (m/z 456 and 385, respectively), indicating structures that were cross-linked off the Asn residue and involved oxygen atom transfer onto the nitrile imine group. Cross-linking in the m/z 608 ion was corroborated by the presence of the m/z 537 ion due to the loss of [Ala]. It is noteworthy that although the m/z 608 ions from (NAAA-*tet*-K–N_2 + H)$^+$ (Figure 4c) and (DAAA-*tet*-K–N_2 + H)$^+$ (Figure 2c) had the same elemental composition, their spectra differed, indicating different isomers or mixtures thereof.

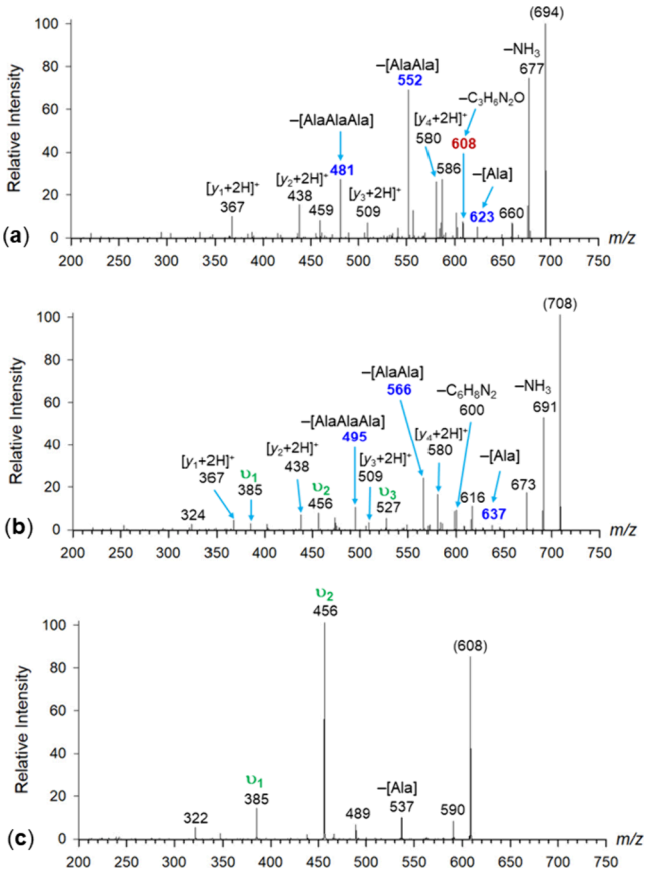

Figure 4. CID-MS^3 spectra of (a) (NAAA-*tet*-K – N_2 + H)$^+$ (m/z 694); (b) QAAA-*tet*-K – N_2 + H)$^+$ (m/z 708). (c) CID-MS^4 spectrum of the m/z 608 ion from Figure 4a.

CID-MS^3 of the Gln ion, (QAAA-*tet*-K–N_2 + H)$^+$ (m/z 708, Figure 4b) also displayed a peak by loss of ammonia (m/z 691), as well as the $[y_n + 2H]^+$ and loss of [Ala] ion series. In addition, the spectrum showed υ_1-υ_3 ions at m/z 385, 456, and 527, that were analogous to those from (EAAA-*tet*-K–N_2 + H)$^+$ (Figure 3c). As discussed above (Scheme 2), the formation of υ_n ions was associated with cross-linking reactions resulting in oxygen transfer to the nitrile-imine group. With (QAAA-*tet*-K–N_2 + H)$^+$, oxygen originated from the carboxamide and peptide amide groups. The role in oxygen transfer of the Asp, Glu, and Gln side chain groups was consistent with previous data on cross-linking in peptide conjugates *N*-terminated with Gly and Ala that lacked reactive side-chain groups and showed no oxygen transfer reactions.

The cross-linking yields in UVPD-MS^2 for NAAA-*tet*-K and QAAA-*tet*-K, 29 and 57%, respectively, closely followed those for DAAA-*tet*-K and EAAA-*tet*-K (Table 1). The CID-MS^3 data for (NAAA-*tet*-K–N_2 + H)$^+$ and (QAAA-*tet*-K–N_2 + H)$^+$ were similar at 72 and 69% respectively. The larger contribution of υ_n ions from (QAAA-*tet*-K–N_2 + H)$^+$ was balanced by the larger fractions of ions due to the loss of [Ala_n] and phenylhydrazine from (NAAA-*tet*-K–N_2 + H)$^+$ (Table 1).

NAAA-*tet*-K and QAAA-*tet*-K Ion Structures and Ion Mobility. The spectra indicated that the polar Asp, Glu, Asn, and Gln side-chain groups participated in cross-linking to the nitrile-imine intermediates in the gas-phase ions. It was of interest to examine the structures of the precursor ions and denitrogenated products to further identify the reactive groups and explore the potential relationships between the precursor

https://doi.org/10.1021/jasms.4c00394
J. Am. Soc. Mass Spectrom. 2025, 36, 175–186

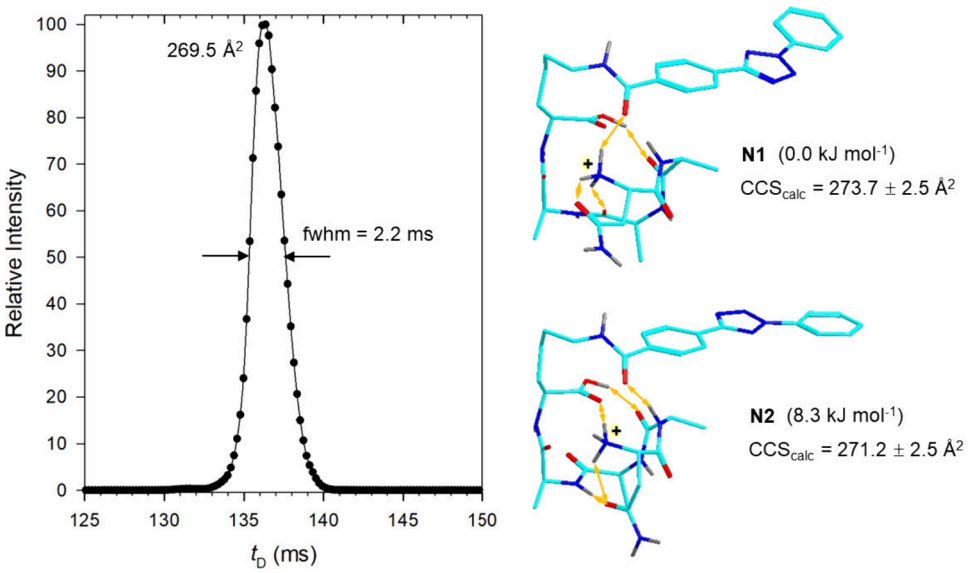

Figure 5. Left panel: Arrival time profile of $(NAAA\text{-}tet\text{-}K + H)^+$ after 5 cycles. Right panel: M06-2X/6-31+G(d,p) optimized the geometries of ions N1 and N2. Atom color coding is as follows: cyan = C, blue = N, red = O, gray = H. Only exchangeable O−H and N−H hydrogens are displayed to avoid clutter. Relative Gibbs energies are from M062X/def2qzvpp single-point energy calculations including B3LYP/6-31+G(d,p) zero-point corrections, and 310 K enthalpies and entropies.

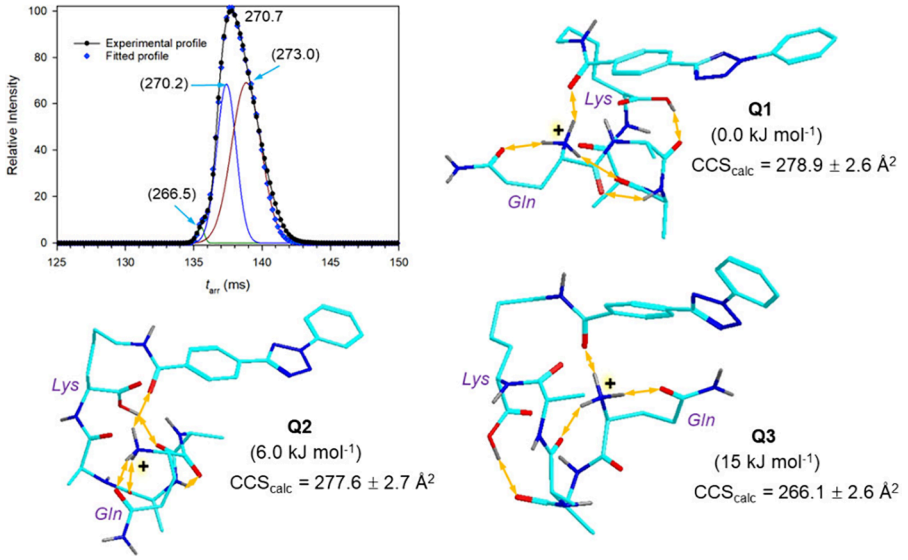

Figure 6. Top left panel: Arrival time profile of $(QAAA\text{-}tet\text{-}K + H)^+$ after 5 cycles with fitted Gaussian peaks and CCS$_{exp}$ in Å^2. M06-2X/6-31+G(d,p) optimized the geometries of ions Q1-Q3. Atom color coding and relative Gibbs energies are given in Figure 5.

and product ion conformations. To that end, we used BOMD and DFT calculations to thoroughly map the conformational space of the precursor ions to establish low-Gibbs energy structures that can be relevant for gas-phase ion populations. For selected $(NAAA\text{-}tet\text{-}K + H)^+$, $(QAAA\text{-}tet\text{-}K + H)^+$, $(NAAA\text{-}tet\text{-}K{-}N_2 + H)^+$, and $(QAAA\text{-}tet\text{-}K{-}N_2 + H)^+$ ions, we also used ion mobility measurements to obtain collision cross sections (CCS$_{exp}$) to be compared with the calculated data (CCS$_{calc}$) to aid structure assignment. Cross-linking in these ion mobility experiments was triggered by CID. As noted above, the CID-MS^3 data of ions generated by UVPD and CID revealed no major differences in the spectra, indicating that these two fragment ion sets were comparable.

The arrival time distribution profile of $(NAAA\text{-}tet\text{-}K + H)^+$ showed a single peak of 2.2 ms full width at half-maximum (fwhm) after 5 cycles (490 cm path length). The measured CCS$_{exp}$ = 269.5 Å^2 was matched by the lowest-Gibbs energy ions N1 and N2 that had CCS$_{calc}$ = 274 and 271 Å^2, respectively (Figure 5). The calculated values differed from the experimental values by only 1.7% and 0.6%, which did not allow us to prioritize N2 over N1. Structures N1 and N2 had a very similar folding pattern of the peptide chain with an internally solvated *N*-terminal ammonium group and developed major hydrogen bonds involving the Lys carboxyl. The main difference distinguishing N1 and N2 was the rotational orientation of the tetrazole ring which was N_2-syn and N_2-anti with respect to the peptide moiety in N1 in N2, respectively (Figure 5).

According to the analysis of the BOMD trajectories, the phenyltetrazole moiety was undergoing a facile rotation about the connecting C−C and N−C bonds, exchanging the N_2-syn and N_2-anti orientations multiple times in the course of 20 ps.

https://doi.org/10.1021/jasms.4c00394
J. Am. Soc. Mass Spectrom. 2025, 36, 175−186

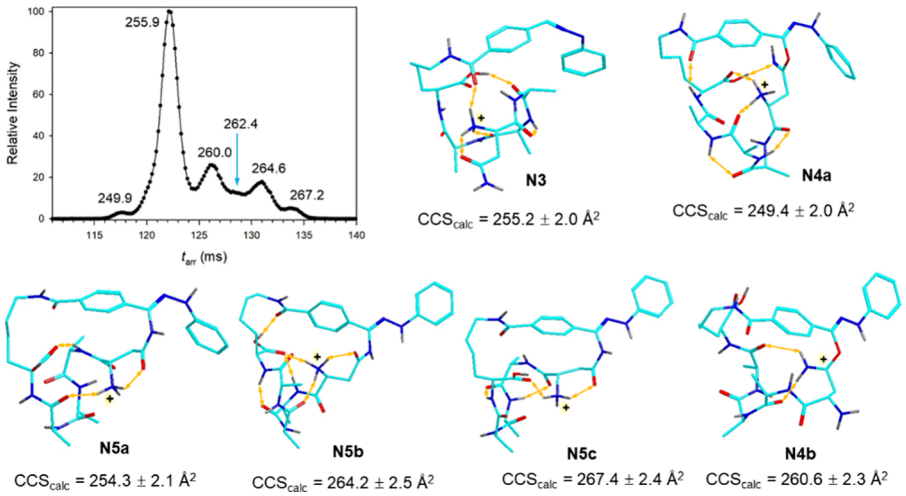

Figure 7. Top left panel: Arrival time profile of $(NAAA\text{-}tet\text{-}K\text{-}N2 + H)^+$ after 5 cycles with CCS_{exp} in Å^2. M06-2X/6-31+G(d,p) optimized the geometries of ions N3-N5b. Atom color coding and relative Gibbs energies are as in Figure 5.

It can be presumed that structures N1 and N2 rapidly interconverted during the ion mobility travel, so that the measured CCS_{exp} was a population-averaged value.

The arrival time distribution profile of $(QAAA\text{-}tet\text{-}K + H)^+$ showed after 5 cycles a broader, unsymmetrical peak that indicated multiple components. The peak maximum was assigned as CCS_{exp} = 270.7 Å^2. Fitting with Gaussian functions gave two major components of CCS_{fit} = 270.2 and 273.0 Å^2 and a more compact minor component with CCS_{fit} = 266.5 Å^2 (Figure 6). The two lowest-Gibbs energy ion structures (Q1 and Q2) had the calculated cross sections at CCS_{calc} = 278.9 and 277.6 Å^2 that were ca. 2.7% larger than the fitted experimental values. A third, more compact component of a higher ΔG_{310} (Q3) had CCS_{calc} = 266.1 Å^2, matching the CCS_{exp} of the minor component in the ion mixture. Structures Q1 and Q2 differed in their folding patterns, which were determined by different hydrogen bonds. In particular, the H-bonding of the Gln amide to the ammonium group in Q2 resulted in a more compact structure than that of Q1 that was reflected by a relatively smaller CCS_{calc} for the former isomer (Figure 6). Structure Q3 had the Gln residue folded toward the diaryltetrazole moiety, resulting in a more compressed structure of a higher energy and smaller CCS_{calc}.

Ion mobility measurements of the CID-generated $(NAAA\text{-}tet\text{-}K\text{–}N_2 + H)^+$ showed multiple components in the arrival time profile that had CCS_{exp} = 249.9, 255.9, 260.0, 264.6, and 267.2 Å^2, with more partially resolved components, as shown in Figure 7. To assign the peaks, we considered several types of structures in our BOMD and DFT computational analysis. Among the nitrile imines, the lowest-energy conformer N3 had CCS_{calc} = 255.2 Å^2 that coincided with the second peak in the arrival time profile. It should be mentioned that nitrile imines were calculated as high-energy intermediates whose presence in the ion mixture was given by kinetic constraints of cyclization and cross-linking. Asn amide O-cross-linked isomers N4a and N4b had CCS_{calc} = 249.4 and 260.6 Å^2, respectively, that coincided with the first and third peak in the arrival time profile. We note that structures of the N4 type were formed by oxygen transfer to the nitrile-imine group and are conducive to the formation of v_n fragment ions upon activation. Another type of Asn amide cross-linked isomers were represented by structures N5. These were the lowest-energy cross-links; e.g., cyclization of N3 to N5c was exergonic by ΔG_{310} = −113 kJ mol^{-1} (Scheme 3). Several N5 structures

Scheme 3. Intermediates and Reaction Enthalpies at 0 K ($\Delta H_{rxn,0}$) for Loss of Phenylhydrazine from $(NAAA\text{-}tet\text{-}K\text{–}N_2 + H)^+$

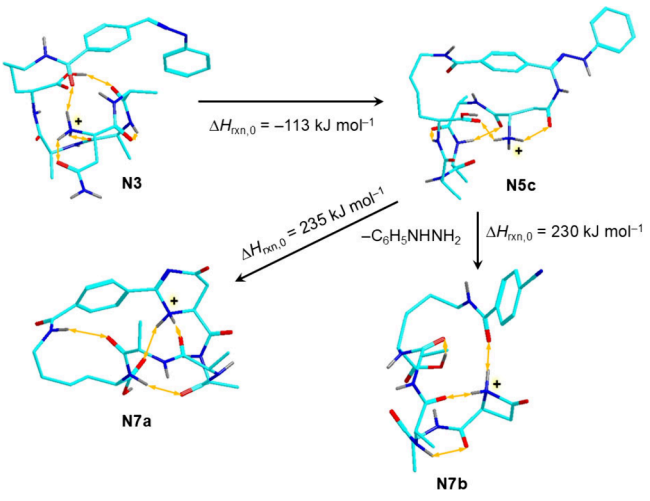

were considered, such as N5a-N5c that had CCS_{calc} close to the CCS_{exp} of the peaks in the arrival time profile (Figure 7). For additional conformers of the N5 type, see N 5d-N 5f (Figure S7, Supporting Information). Structures N5 had strong N–C bonds forming the cross-links and upon excitation were expected to undergo peptide backbone cleavages resulting in [Ala] neutral losses. Another structure type was needed for ions undergoing the loss of $HN{=}CHCH_2CONH_2$ that indicated cross-linking off the Asn residue. These can be represented by structures N6a-N6c in which cross-linking was realized by the Asp-Ala chain amide and was followed by further rearrangement (Figure S7). Similar structures were identified in cross-links of $(GAAA\text{-}tet\text{-}K - N_2 + H)^+$ where their presence was supported by ion mobility and UV-action spectroscopy.[6] According to their CCS_{calc} = 261.1 and 261.9 Å^2 for N6a and N6b, respectively (Figure S7), structures of the N6 type were likely to belong to the minor components of the

https://doi.org/10.1021/jasms.4c00394
J. Am. Soc. Mass Spectrom. 2025, 36, 175−186

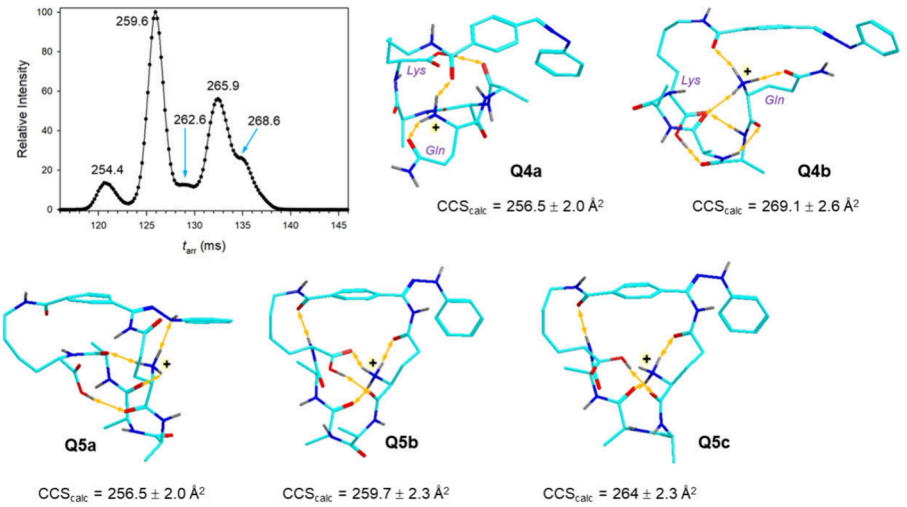

Figure 8. Top left panel: Arrival time profile of (QAAA-*tet*-K−N_2 + H)$^+$ after 5 cycles with CCS$_{exp}$ in Å^2. M06-2*X*/6-31+G(d,p) optimized geometries of ions Q4a, Q4b, and Q5a, Q5b, and Q5c. Atom color coding is as in Figure 5.

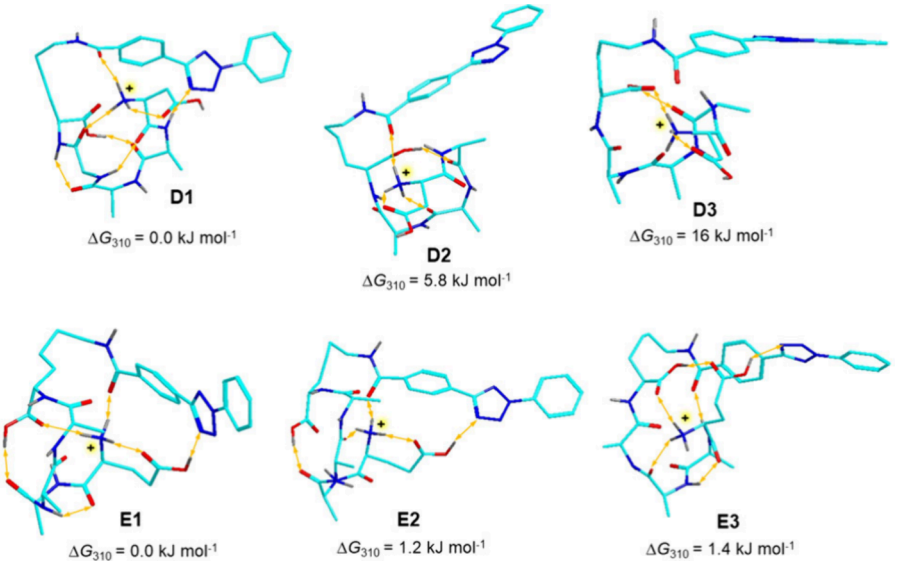

Figure 9. M06-2*X*/6-31+G(d,p) optimized structures of low-energy (DAAA-*tet*-K + H)$^+$ and (EAAA-*tet*-K + H)$^+$ ions. Relative Gibbs energies in each set are from M076−2X/def2qzxvpp single point energy calculations and include zero-point energy corrections, enthalpies, and entropies. Atom color coding is as in Figure 5.

cross-linked products, as shown in the arrival time profile (Figure 7).

Having obtained the energies of (NAAA-*tet*-K−N_2 + H)$^+$ ions, we were able to assess the energetics of some of the less usual dissociations of the cross-linked ions. Scheme 3 shows the M06-2X/def2qzvpp energy, corrected for zero-point vibrational terms, for ring closure in nitrile imine N3, forming the lowest-energy cross-link N5c. The ring closure was exothermic at 113 kJ mol^{-1}, virtually preventing reverse ring opening to the nitrile imine. Ion N5c, which retained the N−*N*-phenyl linkage, was the presumed precursor for the loss of phenylhydrazine that required dissociation of the C−N bond and transfer of two hydrogen atoms onto the leaving group. Several product peptide ions were considered for the phenylhydrazine loss fragment ion, having cyclized structures. In N7a, cyclization involved the N-terminal amine group, forming the protonated amidine ring (Scheme 3). In N7b, the cross-linking N−C bond was disrupted as a result of the phenyl hydrazine loss, forming a nitrile that contained the original Asp side-chain amide nitrogen in the CN group. The exposed Asn side-chain carbonyl then cyclized with the N-terminal amine, forming a four-membered lactam ring. The salient feature of these cyclization-involving dissociations was that the calculated threshold energies (230−235 kJ mol^{-1}, Scheme 3) were comparable to those for typical peptide backbone cleavages that have been reported ranging between 162 and 263 kJ mol^{-1}.[36−39] This was consistent with the observed competition between the two types of ion dissociations (Figure 4, Figure S6a).

Multiple isomers were also observed for the arrival time distribution of (QAAA-*tet*-K−N_2 + H)$^+$ ions produced by CID of (QAAA-*tet*-K + H)$^+$, giving peaks at CCS$_{exp}$ = 254.4, 259.6, 262.6, 265.9, and 268.6 Å^2 (Figure 8). Our survey of optimized structures for the (QAAA-*tet*-K−N_2 + H)$^+$ ions revealed nitrile imines Q4a and Q4b of the respective CCS$_{calc}$ = 256.5 and 269.1 Å^2, matching the first and fifthpeak, respectively, in the arrival time distribution. Regarding cyclic structures, ions Q5a-Q5c were isomers cross-linked by the Gln amide that were

https://doi.org/10.1021/jasms.4c00394
J. Am. Soc. Mass Spectrom. 2025, 36, 175−186

34−65 kJ mol^{-1} more stable than lowest-energy nitrile imine Q4b. That the less stable nitrile imines were detected in the ion mixture pointed to kinetic constraints to cross-linking cyclization. The amide-N-linked structures showed CCS_{calc} = 256.5, 259.7, and 264.0 Å^2 which were close to the CCS_{exp} of the first through fourth peaks in the arrival time distribution (Figure 8). The amide-N-linked structures were considered to be representative of the fraction of (QAAA-*tet*-K−N_2 + H)$^+$ ions that underwent loss of internal [Ala] which was the dominant dissociation on collisional activation (Figure 4b).

DAAA-*tet*-K and EAAA-*tet*-K Ion Structures. The CID-MS^3 spectra of (DAAA-*tet*-K − N_2 + H)$^+$ and (EAAA-*tet*-K − N_2 + H)$^+$ showed a series of fragment ions indicating mixtures of nitrile-imine and cross-linked structures of different types (Figure 1c and 1c, respectively). An important general question regarding nitrile-imine cross-linking was whether the conjugate precursor ion conformation can be related to the formation and composition of the cross-links. Our previous analysis of peptide-nitrile imine scaffolds indicated that cross-linking was governed by the ion dynamics rather than initial static ion structures.[7] We now tested this hypothesis by obtaining and comparing low-energy structures for (DAAA-*tet*-K + H)$^+$ and (EAAA-*tet*-K + H)$^+$ that according to the spectra gave a similar composition of cross-links on UVPD-MS^2 and CID-MS^3. The fully optimized structures of the lowest energy conformers are shown in Figure 9. The lowest-energy (DAAA-*tet*-K + H)$^+$ ion D1 showed the peptide moiety folded on itself, and its conformation was held by multiple hydrogen bonds. The Asp carboxyl oxygens were moderately remote, d(C−O) = 5.5 Å at the closest approach, from the incipient nitrile imine carbon that was the presumed center of nucleophilic attack in the nitrile imine. The position of the diaryltetrazole with respect to the peptide was controlled by two hydrogen bonds, one between the N-terminal NH_3 charged group and the aryl amide C = O, and the other between a tetrazole nitrogen and the Asp amide NH. The other low energy structures, D2 and D3, had even longer distances for the Asp carboxyl oxygens at d(C−O) = 10.4 and 8.8 Å, respectively (Figure 9). In contrast, all the lowest-energy (EAAA-*tet*-K + H)$^+$ ions, E1-E3, showed close proximity of the Glu carboxyl oxygens to the future nitrile-imine carbon at d(C−O) = 3.7, 3.7, and 3.3 Å, respectively. These features were due to a favorable hydrogen bond of the Glu COOH to the tetrazole ring nitrogen atoms (Figure 9) that was enabled by the longer Glu side chain. Hence, it would seem that the (EAAA-*tet*-K + H)$^+$ ions had a higher propensity for cross-linking by the Glu carboxyl. The Table 1 data for UVPD-MS^2 showed that (EAAA-*tet*-K + H)$^+$ produced a significantly higher yield of cross-links, as judged by the prominent v_n fragment ions (Figure 3b) that involved O−C bond to the nitrile imine.

CONCLUSIONS

The results of this combined experimental and computational study allowed us to arrive at the following conclusions. Nitrile-imine intermediates were efficiently produced by UVPD or CID of peptide-tetrazole conjugates containing N-terminal Asp, Glu, Asn, and Gln residues. The nitrile imine formation by loss of N_2 from the tetrazole ring was found to be a facile dissociation of a low threshold energy that competed with peptide backbone cleavages and was particularly promoted by photoexcitation. Asp, Glu, Asn, and Gln side chains participated in covalent bonding to the nitrile imine group, forming cyclized cross-links, with yields reaching 83%. The carboxyl groups in Asp and Glu reacted with the nitrile imines as nucleophiles following proton transfer and formation of the O=C−O−C bonds. The side-chain amide groups in Asn and Gln reacted to form new CONH−C bonds with the nitrile-imine carbon atom. Upon collisional activation, the cyclized products dissociated by two major pathways. One was cleavage of the peptide amide bonds, resulting in the ejection of neutral internal amino acid residues [Ala], [AlaAla], and [AlaAlaAla]. The other pathway commenced by proton-promoted dissociation of the cross-linking O=C−O−C bond, retaining the former carboxyl oxygen and two hydrogen atoms in the nitrile imine, that was followed by standard peptide amide bond dissociations leading to modified C-terminal sequence fragment ions. Another specific dissociation promoted by cross-linking to nitrile imines was the loss of phenylhydrazine. These specific reactions allowed us to distinguish the linear and cyclized peptide products and assess the cross-linking yields. The presented results further expand the range of amino acid residues that undergo cyclization with nitrile-imines and point to the possibility of peptide-nitrile-imine cross-linking being a general feature of gas-phase ions. Further types of residues, such as basic Arg, Lys, and His, hydroxylated Ser and Thr, and aromatic Phe, Tyr, and Trp, need to be investigated regarding their cross-linking reactivity to establish the general applicability of this novel reaction.

ASSOCIATED CONTENT

Supporting Information

The Supporting Information is available free of charge at https://pubs.acs.org/doi/10.1021/jasms.4c00394.

Supplementary tables of high-resolution data, tandem mass spectra, auxiliary optimized ion structures (PDF)

AUTHOR INFORMATION

Corresponding Authors

František Tureček − *Department of Chemistry, Bagley Hall, Box 351700, University of Washington, Seattle, Washington 98195-1700, United States;* orcid.org/0000-0001-7321-7858; Email: turecek@uw.edu

Karel Lemr − *Department of Analytical Chemistry, Faculty of Science, Palacký University, Olomouc 77900, Czech Republic; Institute of Microbiology of the Czech Academy of Sciences, Prague 14220, Czech Republic;* orcid.org/0000-0003-3158-0637; Email: karel.lemr@upol.cz

Authors

Mikuláš Vlk − *Department of Chemistry, Bagley Hall, Box 351700, University of Washington, Seattle, Washington 98195-1700, United States; Institute of Organic Chemistry and Biochemistry, Czech Academy of Sciences, Prague 16610, Czech Republic; Department of Analytical Chemistry, Faculty of Science, Charles University, Prague 12800, Czech Republic;* orcid.org/0000-0002-4695-0584

Jiahao Wan − *Department of Chemistry, Bagley Hall, Box 351700, University of Washington, Seattle, Washington 98195-1700, United States*

Marianna Nytka − *Department of Analytical Chemistry, Faculty of Science, Palacký University, Olomouc 77900, Czech Republic;* orcid.org/0000-0002-9242-8295

Tuan Ngoc Kim Vu − *Department of Chemistry, Bagley Hall, Box 351700, University of Washington, Seattle, Washington 98195-1700, United States*

https://doi.org/10.1021/jasms.4c00394
J. Am. Soc. Mass Spectrom. 2025, 36, 175−186

Complete contact information is available at:
https://pubs.acs.org/10.1021/jasms.4c00394

Notes

The authors declare no competing financial interest.

■ ACKNOWLEDGMENTS

Research at the University of Washington was supported by the Chemistry Division of the U.S. National Science Foundation, Grant CHE-2347921. F.T. acknowledges support by the Klaus and Mary Ann Saegebarth Endowment. M.V. acknowledges support from the Charles University research project SVV260690. Research at Palacký University was supported by projects IGA PrF 2023 027 and IGA PrF 2024 026.

■ REFERENCES

(1) Sharp, J. T. Nitrile Ylides and Nitrile Imines. In *Chemistry of Heterocyclic Compounds 59: Synthetic Applications of 1,3-Dipolar Cycloaddition Chemistry Toward Heterocycles and Natural Products*; Padwa, A.; Pearson, W. H., Eds.; John Wiley & Sons: New York, 2002.
(2) Shawali, A. S. Reactions of Heterocyclic Compounds with Nitrilimines and Their Precursors. *Chem. Rev.* **1993**, *93*, 2731−2777.
(3) Herner, A.; Marjanovic, J.; Lewandowski, T. M.; Marin, V.; Patterson, M.; Miesbauer, L.; Ready, D.; Williams, J.; Vasudevan, A.; Lin, Q. 2-Aryl-5-carboxytetrazole as a New Photoaffinity Label for Drug Target Identification. *J. Am. Chem. Soc.* **2016**, *138*, 14609−14615.
(4) Tian, Y.; Jacinto, M. P.; Zeng, Y.; Yu, Z.; Qu, J.; Liu, W. R.; Lin, Q. Genetically Encoded 2-Aryl-5-carboxytetrazoles for Site-Selective Protein Photo-Cross-Linking. *J. Am. Chem. Soc.* **2017**, *139*, 6078−6081.
(5) Zhang, J.; Liu, J.; Li, X.; Ju, Y.; Li, Y.; Zhang, G.; Li, Y. Unexpected Cyclization Product Discovery from the Photoinduced Bioconjugation Chemistry between Tetrazole and Amine. *J. Am. Chem. Soc.* **2024**, *146*, 2122−2131.
(6) Wan, J.; Nytka, M.; Vu, K.; Qian, H.; Lemr, K.; Turecek, F. Nitrile Imines as Peptide and Oligonucleotide Photocrosslinkers in Gas-Phase Ions. *J. Am. Soc. Mass Spectrom.* **2024**, *35*, 344−356.
(7) Zhu, H.; Nytka, M.; Vu, T. N. K.; Lemr, K.; Tureček, F. Photochemical and Collision-Induced Crosslinking in Stereochemically Distinct Scaffolds of Peptides and Nitrile Imines in Gas-Phase Ions. *J. Am. Soc. Mass Spectrom.* **2024**, DOI: 10.1021/jasms.4c00317.
(8) Tureček, F. Covalent Crosslinking in Gas-Phase Biomolecular Ions. An Account and Perspective. *Phys. Chem. Chem. Phys.* **2023**, *25*, 32292−32304.
(9) Swenson, C. S.; Mandava, G.; Thomas, D. M.; Moellering, R. E. Tackling Undruggable Targets with Designer Peptidomimetics and Synthetic Biologics. *Chem. Rev.* **2024**, DOI: 10.1021/acs.chemrev.4c00423.
(10) Dove, J. E.; Hippler, H.; Troe, J. Direct Study of Energy Transfer of Vibrationally Highly Excited Carbon Disulfide Molecules. *J. Chem. Phys.* **1985**, *82*, 1907−1919.
(11) Heymann, M.; Hippler, H.; Troe, J. Collisional Deactivation of Vibrationally Highly Excited Polyatomic Molecules. IV. Temperature Dependence of ⟨ΔE⟩. *J. Chem. Phys.* **1984**, *80*, 1853−1860.
(12) Pepin, R.; Tureček, F. Kinetic Ion Thermometers for Electron Transfer Dissociation. *J. Phys. Chem. B* **2015**, *119*, 2818−2826.
(13) Dang, A.; Korn, J. A.; Gladden, J.; Mozzone, B.; Tureček, F. UV-Vis Photodissociation Action Spectroscopy on Thermo LTQ-XL ETD and Bruker amaZon Ion Trap Mass Spectrometers: A Practical Guide. *J. Am. Soc. Mass Spectrom.* **2019**, *30*, 1558−1564.
(14) Giles, K.; Ujma, J.; Wildgoose, J.; Pringle, S.; Richardson, K.; Langridge, D.; Green, M. A Cyclic Ion Mobility-Mass Spectrometry System. *Anal. Chem.* **2019**, *91*, 8564−8573.
(15) Berendsen, H. J. C.; Postma, J. P. M.; van Gunsteren, W. F.; DiNola, A.; Haak, J. R. Molecular Dynamics with Coupling to an External Bath. *J. Chem. Phys.* **1984**, *81*, 3684−3690.
(16) Řezáč, J.; Fanfrlík, J.; Salahub, D.; Hobza, P. Semiempirical Quantum Chemical PM6Method Augmented by Dispersion and H Bonding Correction Terms Reliably Describes Various Types of Noncovalent Complexes. *J. Chem. Theory Comput.* **2009**, *5*, 1749−1760.
(17) Řezáč, J. Cuby: An Integrative Framework for Computational Chemistry. *J. Comput. Chem.* **2016**, *37*, 1230−1237.
(18) Stewart, J. J. P. *MOPAC 16*; Stewart Computational Chemistry: Colorado Springs, CO, 2016.
(19) Becke, A. D. Density-Functional Exchange-Energy Approximation with Correct Asymptotic Behavior. *Phys. Rev. A* **1988**, *38*, 3098−3100.
(20) Grimme, S.; Ehrlich, S.; Goerigk, L. Effect of the Damping Function in Dispersion Corrected Density Functional Theory. *J. Comput. Chem.* **2011**, *32*, 1456−1465.
(21) Nickerson, C. J.; Bryenton, K. R.; Price, A. J. A.; Johnson, E. R. Comparison of Density-Functional Theory Dispersion Corrections for the DES15K Database. *J. Phys. Chem. A* **2023**, *127*, 8712−8722.
(22) Zhao, Y.; Truhlar, D. G. The M06 Suite of Density Functionals for Main Group Thermochemistry, Thermochemical Kinetics, Noncovalent Interactions, Excited States, and Transition Elements: Two New Functionals and Systematic Testing of Four M06-Class Functionals and 12 Other Functionals. *Theor. Chem. Acc.* **2008**, *120*, 215−241.
(23) Weigend, F. Accurate Coulomb-Fitting Basis Sets for H to Rn. *Phys. Chem. Chem. Phys.* **2006**, *8*, 1057−1065.
(24) Singh, U. C.; Kollman, P. A. An Approach to Computing Electrostatic Charges for Molecules. *J. Comput. Chem.* **1984**, *5*, 129−145.
(25) Besler, B. H.; Merz, K. M., Jr; Kollman, P. Atomic Charges Derived from Semiempirical Methods. *J. Comput. Chem.* **1990**, *11*, 431−439.
(26) Ieritano, C.; Crouse, J.; Campbell, J. L.; Hopkins, W. S. A Parallelized Molecular Collision Cross Section Package with Optimized Accuracy and Efficiency. *Analyst* **2019**, *144*, 1660−1670.
(27) Ieritano, C.; Hopkins, W. S. Assessing Collision Cross Section Calculations Using MobCal-MPI with a Variety of Commonly Used Computational Methods. *Mater. Today Commun.* **2021**, *27* (102226), 102226.
(28) Chu, I. K.; Siu, C.-K.; Lau, J. K.-C.; Tang, W. K.; Mu, X.; Lai, C. K.; Guo, X.; Wang, X.; Li, N.; Yao, Z.; Xia, Y.; Kong, X.; Oh, H.-B.; Ryzhov, V.; Tureček, F.; Hopkinson, A. C.; Siu, K. W. M. Proposed Nomenclature for Peptide Ion Fragmentation. *Int. J. Mass Spectrom.* **2015**, *390*, 24−27.
(29) Roepstorff, P.; Fohlman, J. Proposal for a Common Nomenclature for Sequence Ions in Mass Spectra of Peptides. *Biomed. Mass Spectrom.* **1984**, *11*, 631.
(30) Bleiholder, C.; Osburn, S.; Williams, T. D.; Suhai, S.; Van Stipdonk, M.; Harrison, A. G.; Paizs, B. Sequence-Scrambling Fragmentation Pathways of Protonated Peptides. *J. Am. Chem. Soc.* **2008**, *130*, 17774−17789.
(31) Novák, J.; Lemr, K.; Schug, K. A.; Havlíček, V. CycloBranch: De Novo Sequencing of Nonribosomal Peptides from Accurate Product Ion Mass Spectra. *J. Am. Soc. Mass Spectrom.* **2015**, *26*, 1780−1786.
(32) Ly, T.; Julian, R. R. Residue-Specific Radical-Directed Dissociation of Whole Proteins in the Gas Phase. *J. Am. Chem. Soc.* **2008**, *130*, 351−358.
(33) Tureček, F.; Julian, R. R. Peptide Radicals and Cation-Radicals in the Gas Phase. *Chem. Rev.* **2013**, *113*, 6691−6733.
(34) Zhang, L.; Reilly, J. P. Peptide de Novo Sequencing Using 157 nm Photodissociation in a Tandem Time-of-Flight Mass Spectrometer. *Anal. Chem.* **2010**, *82*, 898−908.
(35) Brodbelt, J. S. Photodissociation Mass Spectrometry: New Tools for Characterization of Biological Molecules. *Chem. Soc. Rev.* **2014**, *43*, 2757−2783.

(36) Klassen, J. S.; Kebarle, P. Collision-Induced Dissociation Threshold Energies of Protonated Glycine, Glycinamide, and Some Related Small Peptides and Peptide Amino Amides. *J. Am. Chem. Soc.* **1997**, *119*, 6552−6563.
(37) Paizs, B.; Suhai, S. Fragmentation Pathways of Protonated Peptides. *Mass Spectrom. Rev.* **2005**, *24*, 508−548.
(38) Laskin, J.; Yang, Z.-B.; Song, T.; Lam, C.; Chu, I. K. Effect of the Basic Residue on the Energetics, Dynamics, and Mechanisms of Gas-Phase Fragmentation of Protonated Peptides. *J. Am. Chem. Soc.* **2010**, *132*, 16006−16016.
(39) Mookherjee, A.; Armentrout, P. B. Thermodynamics and Reaction Mechanisms for Decomposition of a Simple Protonated Tripeptide, H^+GGA: From H^+ GGG to H^+GAG to H^+GGA. *J. Am. Soc. Mass Spectrom.* **2022**, *33*, 355−368.

https://doi.org/10.1021/jasms.4c00394
J. Am. Soc. Mass Spectrom. 2025, 36, 175−186